ADVANCED FUNCTIONAL MATERIALS
www.afm-journal.de

Materials Views
www.MaterialsViews.com

Enhanced and Engineered d^0 Ferromagnetism in Molecularly-Thin Zinc Oxide Nanosheets

Takaaki Taniguchi, Kazuhiro Yamaguchi, Ayako Shigeta, Yuki Matsuda, Shinya Hayami, Tetsuya Shimizu, Takeshi Matsui, Teruo Yamazaki, Asami Funatstu, Yukihiro Makinose, Nobuhiro Matsushita, Michio Koinuma, and Yasumichi Matsumoto*

Molecularly-thin nanosheets are ultimate two-dimensional (2D) nanomaterials potentially giving unusual physical and chemical properties due to the strong 2D quantum and surface effects. Here, it is demonstrated that 1.5-nm-thick ZnO nanosheets exhibit greatly enhanced room-temperature ferromagnetism. Saturation magnetization value of the nanosheets with intercalated dodecyl sulfate layers is approximately 100 times that of ZnO mesocrystals. Anion exchange with dodecyl phosphate layers strongly suppresses ferromagnetic ordering as a result of surface defect passivation while maintaining bulk-like n-type semiconducting properties, which reveals significance of interfacial states to engineer functional properties of nanosheet-based hybrid materials.

1. Introduction

Nanostructured materials potentially exhibit distinctly different physical and chemical properties from the bulk owing to the high surface to volume ratio and alternation in the electronic states. So far, unique nanosize-effects such as quantum effects,[1] surface plasmon resonance,[2] and metastable-phase stabilization[3] have contributed significantly to rapid progress of studies in fields of nanoscience and nanotechnology. Recently, a novel size effect relating magnetic properties has been revealed, that is, diamagnetic materials in the bulk state can exhibit ferromagnetism by downsizing into nanodimensions. For examples, gold nanoparticles[4,5] and graphene nanoribbons[6–8] present ferromagnetic behavior owing to the presence of surface polarization and zigzag edges, respectively. In addition, recent studies ruled out that nanostructured metal oxides exhibit RT ferromagnetism in absence of magnetic impurities at RT.[9–11] Although the origin of so-called "d^0 ferromagnetism" is still debatable, it is highly probable that surface states have played a role in inducing ferromagnetic order owing to enhanced d^0 ferromagnetic localization at surface.[11–17] Organic and inorganic ferromagnetic materials engineered without transition metal (TM) ions are potential candidates for generating novel spintronics devices. Therefore, understanding and controlling d^0 ferromagnetism are very important for future developments in the field of spintronics.

Because of the excellent and multifunctional properties, d^0 ferromagnetism in ZnO nanostructures has been investigated most intensively among metal oxides.[13–16,18–29] However, in general, d^0 ferromagnetism observed in ZnO nanomaterials is weak: for example, Ms values measured for ZnO nanocrystals and nanorods were reported to be in the range of -10^{-3}–10^{-6} emu/g,[23,27] and at these levels, subtraction of the diamagnetic response is often required to clearly observe ferromagnetic behavior. This indicates that the volume fraction of the diamagnetic core is so large even in nanoscale materials that the magnetic response from the tiny surface ferromagnetic region is very weak. Therefore, if the surface components could be excised exclusively and accumulated in bulk quantities, it might be possible to substantially enhance the ferromagnetic response from undoped ZnO to prove the origin of the d^0 ferromagnetism. This idea motivated us to study the magnetic properties of molecularly thin ZnO single-crystalline nanosheets.

2. Results and Discussion

2.1. Structural and Magnetic Properties of the ZnO NS-DS Hybrid

In our previous study,[30] we demonstrated the synthesis of single-crystalline ZnO nanosheets with a wurtzite structure

Dr. T. Taniguchi, K. Yamanguchi, A. Shigeta, Y. Matsuda, Prof. S. Hayami, T. Shimizu, T. Matsui, A. Funatsu, Dr. M. Koinuma, Prof. Y. Matsumoto
Graduate School of Science and Technology
Kumamoto University
2-39-1 Kurokami, Chuo-ku, Kumamoto, 860-8555, Japan
E-mail: takatani@gpo.kumamoto-u.ac.jp
Dr. T. Taniguchi, Prof. S. Hayami, Dr. M. Koinuma, Prof. Y. Matsumoto
JST, CREST, 5 Sanbancho, Chiyoda-ku, Tokyo, 102-0075, Japan
Dr. T. Yamazaki
Department of Physics
Faculty of Science and Technology
Tokyo University of Science
2461 Yamazaki, Noda, Chiba 278-8510, Japan
Y. Makinose, Prof. N. Matsushita
Materials and Structures Laboratory
Tokyo Institute of Technology
4259 Nagatsuta, Midori-ku, Yokohama 226-8503, Japan

DOI: 10.1002/adfm.201202704

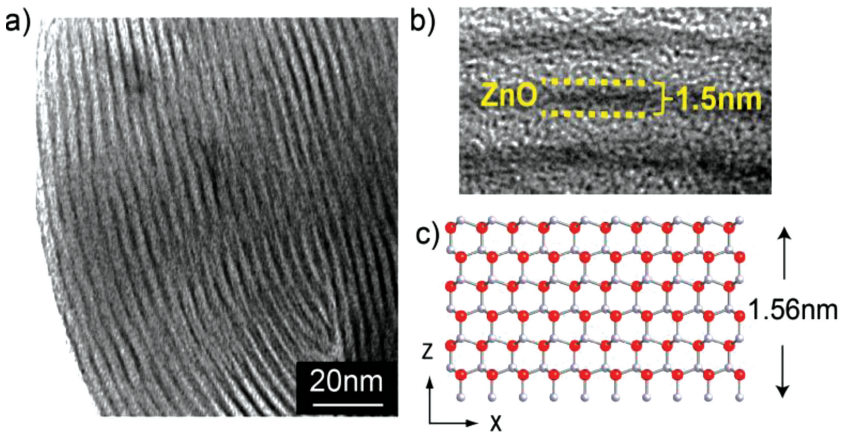

Figure 1. a) Low-and b) high- magnification TEM images of ZnO nanosheets with intercalated DS anions. c) Cross-sectional view of three unit-cell ZnO nanosheets with (0001) and (000$\bar{1}$) surfaces. Red and gray balls correspond to oxygen and zinc ions, respectively.

exhibiting (0001) and (000$\bar{1}$) surfaces by an electrochemical-decomposition method using the dodecyl sulfate (DS) anion as a structure-directing agent. **Figure 1**a shows a typical cross-sectional transmission microscopy (TEM) image of ZnO nanosheet layers intercalated with DS layers. Figure 1b presents that the lamellar structure is composed of alternating layers of approximately 1.5-nm-thick ZnO sheets (dark) and 2-nm-thick DS bilayers (bright). According to first-principle calculations, there is a driving force for transforming wurtzite crystal structures to graphitic structures for thin nanoplates with (0001) and (000$\bar{1}$) surfaces, in which the thickness is less than ≈5 nm.[28,31,32] In contrast, our study revealed that organic layers could stabilize the wurtzite structure, allowing the formation of 1.5-nm-thick ZnO nanosheets in which the thickness is well below the critical value theoretically predicted. Note that we could not obtain a lattice image of the nanosheet layers because the electron beam accelerated at 200 keV immediately decomposed the layered structure leading to nucleation of nanoparticles (see Supporting Information Figure S1), which indicated that these nanosheets were less stable than the ZnO bulk and conventional nanocrystals toward electron beam irradiation. The thickness (1.5 nm) is approximately three times that of the lattice constant along c axis (0.52 nm; Figure 1c). In this structural mode, a fraction of the Zn atoms (2/7) are located in the outermost Zn layers; therefore, the extremely thin nanosheets ultimately form a two-dimensional architecture, which enhances surface ferromagnetic properties.

Figure 2a shows an HM curve of ZnO nanosheet-DS (ZnO NS-DS) lamellar hybrid and reference samples (ZnO mesocrystals and microrods). ZnO nanosheets demonstrated clear ferromagnetic behavior at RT exhibiting the Ms value of 0.04 emu/g (ZnO) and coercivity of 50 Oe with a negligibly small diamagnetic signal. The Ms value is one and two order larger than 3.2-nm and 10-nm ZnO nanocrystals reported previously.[16,27] Note that we employed 41.71 mg ZnO NS-DS power for SQUID measurements to obtain large Ms value (ca. 1×10^{-3} emu as raw data) so that the remarkably high Ms value of the nanosheets was measured precisely. Figure 2b displays the zero-field-cooled (ZFC) and field-cooled (FC) magnetization curves of the ZnO nanosheets at the dc field of 500 Oe. The ZFC and FC curves show distinct splitting up to 300 K, which confirms a Curie temperature of the sample is higher than RT. No magnetic phase transition was observed in the measured temperature range, which indicates that there is no ferromagnetic contaminants exhibiting a Curie temperature lower than 300 K in the sample.

On the other hand, ZnO sample (mesocrystals, 200 nm in average particle size) synthesized by the electrodeposition method using the same zinc source and reaction temperature without SDS displayed dominant diamagnetic behavior (Figure 2a). Although a weak ferromagnetic response was observed in the sample (Figure 2c), the Ms value was approximately one-hundredth that of the nanosheet-sample. TEM image shows that the sample exhibited a porous-like structure, while the electron diffraction (ED) spots were slightly elongated due to the presence of a small lattice mismatch (Figure 2d). These features are typical of mesocrystals composed of grains connected with slightly different orientations.[33] The mesocrystalline structure could produce detectable ferromagnetic signal

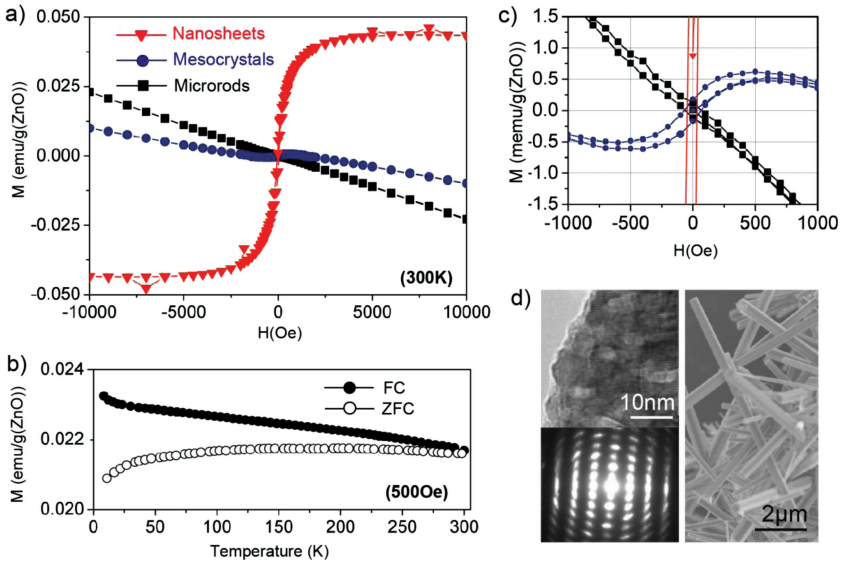

Figure 2. a,c) *M–H* curves of ZnO nanosheets, mesocrystals, and microrods at room temperature. Note that amount of ZnO in ZnO NS-DS hybrid sample was obtained by TG data (44 wt%), and then the value was used to produce the MH curve for 1 g of ZnO. b) FC-ZFC magnetization curve of ZnO nanosheets in external magnetic field of 500 Oe. d) HRTEM image and ED pattern of ZnO mesocrystals (left), and SEM image of ZnO microrods (right).

due to the relatively large surface (interface) to volume ratio. Considering that the nanosheets and mesocrystals were synthesized by the electrochemical deposition method, these samples might exhibit a similar defect concentration in the bulk, which further supports that the large Ms of nanosheets was due to the extremely thin thickness. Note that ZnO hexagonal microrods with a lower surface to volume ratio resulted in negligible ferromagnetic response (Figure 2a,d), which supports well that nanostructures played a crucial role to produce d^0 ferromagnetism rather than the presence of magnetic impurities.

We confirmed that the levels of magnetic-transition metals, such as Fe, Co, and Ni, are below the detection sensitivity limit for the inductively coupled plasma (ICP) analysis (10 ppm) in both the initial materials [$Zn(NO_3)_2$ and SDS] and the synthesized samples. EDX analysis supported that the samples were free from magnetic impurities (data not shown). We also confirmed that $Zn(NO_3)_2$ and SDS exhibit diamagnetic properties at 2 and 300 K (see Supporting Information Figure S3). Moreover, annealing of the nanosheets at 1000 °C eliminated FM properties (see Supporting Information Figure S4). These analyses excluded the possibility of a significant contribution from TM impurities to the ferromagnetic signals detected. Thus, the dramatic enhancement of ferromagnetism observed in the nanosheets should be closely related to the extreme thinness of the sheets.

2.2. Optical Properties of ZnO NS-DS Hybrid

The optical properties were investigated to understand the origin of the enhanced RT ferromagnetism observed in the ZnO nanosheets. **Figure 3**a shows the PL spectra of ZnO nanosheets, mesocrystals, and microrods. These spectra display a broad emission band covering the visible region. The broad emission band could be deconvoluted into multiple bands corresponding to different emissions near the blue-green (480–550 nm), yellow (550–610 nm), and orange-red (610–750 nm) regions. Although the origin of defects producing these visible emission bands are still debatable, it is indicated that the green emission originates from the singly charged oxygen vacancy (V^{+}_0), while the yellow one (580 nm) is commonly attributed to the doubly charged oxygen vacancies (V^{++}_0) and the orange-red emission (P3) is associated with the excess oxygen on the ZnO surface (Figure 3c).[23] The strongest bands in the emission spectra of the nanosheets and mesocrystals are the P1 and P2 bands, respectively. These spectral features suggest that V^{+}_0 and V^{++}_0 defects are involved at a high concentration level in nanosheets and mesocrystals, respectively. V^{+}_0 defects with unpaired electrons can be the source of ferromagnetism;[16,18,23,26] namely, V^{+}_0 defect clusters can limit delocalization of unpaired electrons potentially giving rise to ferromagnetic double exchange. Therefore, the strong P1 band observed for the nanosheets indicates that the considerably-enhanced ferromagnetism relate preferred formation of V^{+}_0 defects rather than V^{++}_0 defects at the interface between the nanosheets and DS layers in addition to the extremely high surface to volume ratio due to the molecular thinness. Notably, the PL excitation and UV-vis absorption spectra (Figure 3b) exhibit a band corresponding to band-edge absorption, which is remarkably blue-shifted for the nanosheet sample; the band gap (GB) energy of nanosheets corresponded to 3.5 eV, where the value was 0.5 eV larger than mesocrystals and microrods (Figure S5, Supporting Information). The strong two-dimensional quantum confinement effects suggested that observed ferromagnetism might be also induced by alternation of the band structure giving a asymmetry in the spin distribution.

2.3. Effects of Organic Layer on Magnetic Properties of ZnO NSs

Next, we attempted to control the d^0 ferromagnetism of the ZnO nanosheets by an anion-exchange process. It has already been accepted that capping molecules influence the ferromagnetic properties of the undoped ZnO nanocrystals.[15,19,27] However, the total magnetism was not significantly changed in these cases, as magnetization predominantly derives from diamagnetic behavior within the grain interior. In contrast, molecularly-thin ZnO nanosheets exhibit true ferromagnetism without significant diamagnetism. We expected that intercalation with different molecules would totally alter the interfacial

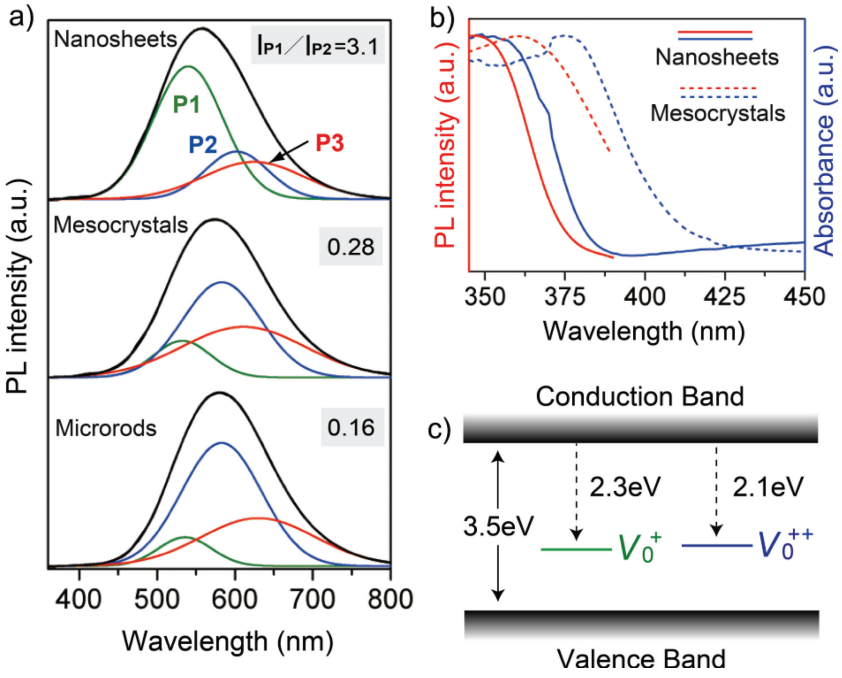

Figure 3. a) PL emission spectra of ZnO nanosheets, mesocrystals and microrods excite at 300 nm. b) UV-vis absorption spectra and PL excitation spectra of ZnO nanosheets and mesocrystals monitored at the emission peak wavelengths. c) Energy diagram of the conduction and valence bands with defect levels of ZnO nanosheet, estimated with PL emission and UV-vis absorption data.

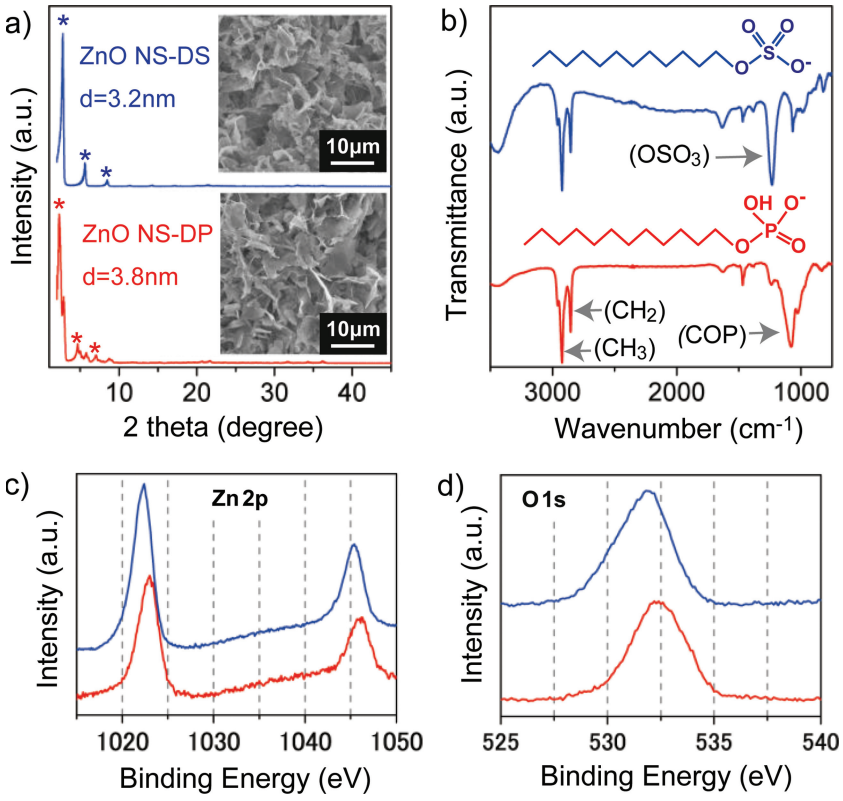

Figure 4. a) SEM images and XRD patterns of ZnO NS-DS and ZnO NS-DP lamellar hybrids; peaks labeled with asterisks were used to calculate inter lamellar spacing. b) IR spectra of ZnO-DS and ZnO NS-DP lamellar hybrids. c) Zn 2P and d) O 1s XP spectra of ZnO NS -DS and ZnO NS-DP lamellar hybrids.

bonding states, thereby impacting the surface magnetism while keeping the molecularly thin thickness.

In an anion-exchange process, ZnO nanosheet–DS lamellar hybrids deposited on an ITO film were immersed in sodium dodecyl phosphate (SDP) for one week at RT. During the process, pealing of the products from the ITO substrate was not observed, and the overall morphology of the products was unchanged (**Figure 4**a). X-ray diffraction (XRD) patterns of ZnO nanosheet–lamellar hybrids before and after the anion-exchange process (Figure 4a) show that the inter-lamellar spacing expanded to 3.8 nm (calculated with reflections labeled with asterisks in Figure 4a) during the process without the formation of Zn-related impurity compounds (see also Supporting Information Figure S6), indicating that the DS anion were exchanged successfully by DP anions. Fourier transform infrared (FT–IR) spectra (Figure 4b) reveal that the initial absorption band at 1235 cm^{-1} from the sulfate group weakened remarkably while the bands at 1075 cm^{-1} from the phosphate group became much stronger.[34,35] The expansion of inter lamellar spacing and the intense IR band form the phosphate group indicates the presence of DP layers sandwiching the nanosheet layers. X-ray photoemission spectroscopy (XPS) showed undetectable S 2p signal for ZnO NS-DP hybrid, while P 1s peaks appeared clearly after the intercalation of DP anions (see Supporting Information, Figure S7). XPS analysis also revealed that positions of Zn 2P and O 1S XP peaks were shifted toward higher energy by the anion exchange (Figure 4c,d), which suggests alternation in the interfacial Zn-O bonding states between nanosheet- and organic-layers.

Photoconductivity (PC) measurements (**Figure 5**a) showed that nanosheets interlaced with DS or DP provided clear anodic photocurrent owing to n-type semiconducting properties, indicating that the overall wurtzite structure of the nanosheet layer was maintained during the anion-exchange process. UV-vis absorption spectra (Figure 5b) show that the anion-exchange process caused no remarkable shift in the absorption edge position. Combination analysis by XPS, UV-vis absorption, and PC measurements revealed that the anion-exchange process changed interfacial bonding states, while it did not remarkably alter the overall crystal and band structure of the nanosheets.

Figure 6a shows an *M–H* curve of the ZnO nanosheets with intercalated DP anions. The figure demonstrates that the ferromagnetic signal is clearly observed after the anion-exchange process; however, the Ms value decreases to be approximately 1/10 as compared with that of the ZnO NS–DS lamellar architecture. Note that the TG data (Supporting Information, Figure S2) showed that the amounts of organic species in ZnO NS-DS and ZnO NS-DP hybrids were close (46 wt% and 49 wt%, respectively), which conformed that the change in ZnO/organic weight-ratio by the anion exchange process contributed insignificantly to the decrease of the Ms value. Importantly, the PL emission spectra (Figure 6b) reveal that the P2 band is stronger than the P1 band for the ZnO nanosheet–DP lamellar hybrid, whereas the trend is the opposite for the DS-intercalated nanosheets (Figure 3a). This indicates that the anion-exchange process induced surface defect

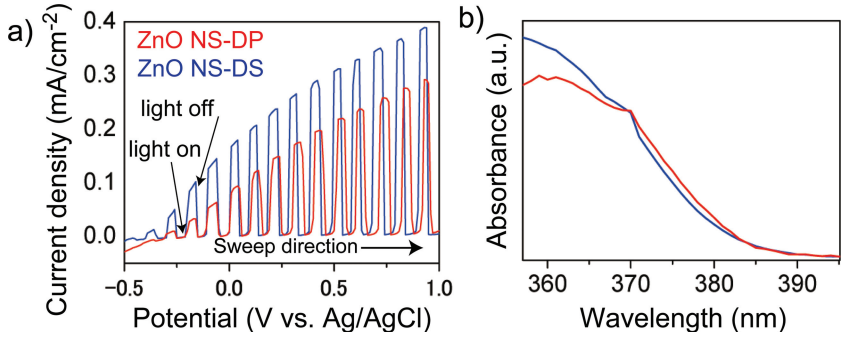

Figure 5. a) Current–potential curve of GO nanosheet electrode under chopped light irradiation. b) UV-vis absorption spectra of ZnO NS-DS and ZnO NS-DP lamellar hybrids.

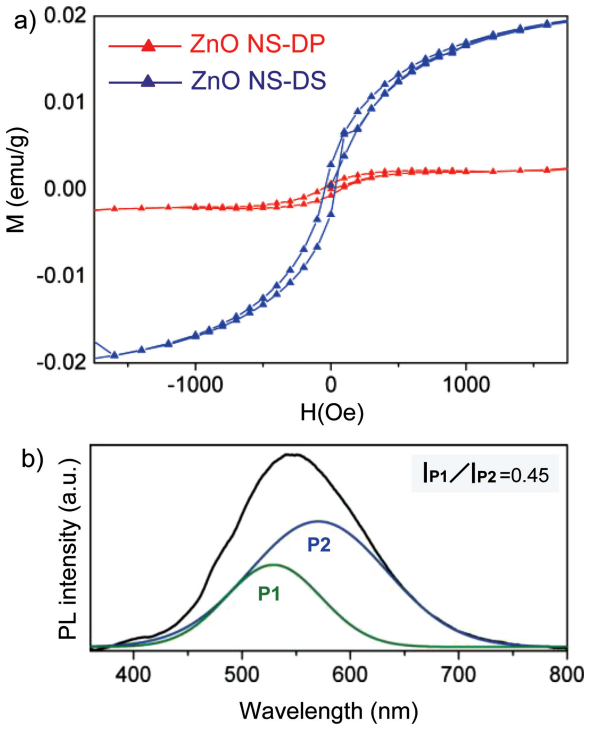

Figure 6. a) *M–H* curves of ZnO NS-DS and ZnO NS-DP lanmellar hybrids. b) PL emission spectra of of ZnO NS-DS and ZnO NS-DP lamellar hybrids excited at 330 nm.

reconstruction. As a result, the relative concentration of V^{++}_0 defects to V^{+}_0 defects increased, thereby suppressing ferromagnetic ordering. Notably, first-principle calculations suggested that the magnetism of the ZnO nanoplates with (0001) and (000$\bar{1}$) surfaces enhanced d^0 ferromagnetism when the thickness was ≈8 nm owing to growing asymmetry in the spin distribution within the distorted bands formed from Zn (3d) and O (2p) orbitals.[28] However, according to our experimental results, the ferromagnetic properties of extremely thin nanosheets with the average thickness of 1.5 nm were significantly influenced by the surface defect states. This result strongly indicates that modification of the band structure resulting from the reduced nanoscale thickness did not significantly contribute to the magnetic properties. To date, theoretical and experimental studies have suggested that many types of defects and surface bonding states, including oxygen vacancy,[23,26] zinc vacancy,[22] chemisorbed oxygen,[12] and Zn–S bonding,[13,14] can afford ferromagnetism. Among these candidates, our experimental results indicate that double exchange among the electrons trapped in V^{+}_0 defect clusters at the nanosheet-organic interface plays a major role in the production of ferromagnetism observed for the ZnO nanosheets, while origin of d^0 may depend on materials and the nanostructures. Therefore, we have concluded that the formation of dense integration of interfacial two-dimensional ferromagnetic centers in the lamellar structure could give dramatically enhanced and tuned ferromagnetism to ZnO nanosheets.

3. Conclusion

In summary, we demonstrated that 1.5-nm-thick ZnO nanosheets exhibit considerably enhanced d^0 ferromagnetism owing to the extremely high surface to volume ratio. PL and anion-exchange studies revealed that the d^0 ferromagnetism originates from the clusters of spin-polarized defects rather than from two-dimensional quantum effects. Our research reveals that molecularly-thin ZnO nanosheets can be engineered to exhibit enhanced or suppressed ferromagnetism while maintaining bulk-like n-type semiconducting properties, a finding that can provide a foundation for designing novel classes of two-dimensional metal–organic hybrid materials with tunable multifunctional properties.

4. Experimental Section

Electrochemical Deposition of ZnO Nanosheets with DS Layers, and ZnO Mesocrystals: The synthetic procedure is presented in detail in ref. [1]. Briefly, the cathodic-electrodeposition process was performed at –1.1 V vs a Ag/AgCl reference electrode for 1 h at 70 °C in an aqueous solution of $Zn(NO_3)_2{\cdot}6H_2O$ and SDS. ITO-coated glass and platinum plates were used as the working and counter electrodes, respectively. ZnO mesocrystals were deposited on a ITO-coated glass in an aqueous solution of $Zn(NO_3)_2{\cdot}6H_2O$ without SDS additive.

Synthesis of ZnO Microdots: 12 mL of 0.1 M hexamethylenetetramine aqueous solution and 2 mL of 0.1 M $Zn(NO_3)_2{\cdot}6H_2O$ aqueous solution were mixed. Then, water and 0.1 M HCl aqueous solution were added to the solution to prepare 100 mL solution with pH of 6. The solution was heated at 90 °C for 24 h. The products (ZnO microrods) were collected by centrifugation (5000 rpm for 30 min) and washed twice with ethanol, and then dried in vacuum at room temperature for 6 h in air.

Synthesis of ZnO Nanosheets with DP Layers by Anion-Exchange: ZnO nanosheets with DS layers deposited on ITO-coated glass were immersed in sodium dodecyl phosphate (SDP) (Tokyo Chemical Industry) was dispersion (0.01 M, 10 mL) for 1 week. Then the sample was washed with water several times, and then dried in vacuum at room temperature.

Characterization: TEM was performed with a Hitachi HF-2000 unit operating at 200 kV. A Quantum Design MPMSXL-5 superconducting quantum interference device (SQUID) magnetometer was used for magnetization measurements. Powder-sample was placed inside the SQUID chamber, and the field dependence of the magnetization was measured at 300 K. For SQUID measures, ZnO NS-DS layers, ZnO NS-DP, or ZnO NCs were removed from the ITO substrates to obtain powder-samples. (ICP) atomic emission spectroscopy was performed using a CID plasma photoemission spectrophotometer (IRIS Advantage, Nippon Jarrell Ash). An HNO_3 aqueous solution was used to dissolve powder-samples. PL spectra were obtained using a spectrofluorometer (Jasco FP-6500) at room temperature. UV-vis absorption spectra were obtained using a spectrometer (Jasco, V-550). Field-emission scanning-electron microscopy (SEM; Hitachi, SU-8000) was performed in secondary electron-imaging mode with the acceleration voltage of 5 kV. The crystal structures were analyzed from their XRD (Rigaku RINT-2500VHF) patterns obtained using Cu Kα radiation (λ = 1.54056 Å). The room temperature infrared (IR) Fourier-transform spectra were recorded on a Jeol JIR-7000 spectrometer. The products (20 mg) were thoroughly ground with 400 mg of potassium bromide powder (KBr for IR, Wako) and subjected to IR analysis. XPS measurements were performed under vacuum (>7–10 Pa) using a spectrometer (Thermo Scientific Sigma Probe) equipped with a monochromatized X-ray source (1486.6 eV). Electrons emitted from the samples were detected by a hemispherical energy analyzer equipped with six channeltrons. The overall energy resolution for XPS was below 0.55 eV (on Ag 3d3/2 with a pass energy of 15 eV). Inductively coupled plasma. The photoelectrochemical properties

of ZnO NS-DS and ZnO NS-DP deposited on an ITO substrate were measured with a three electrode system consisting of working (ZnO/ITO), counter (Pt), and reference (Ag/AgCl) electrodes. A 0.1 M Na_2SO_4 solution in a quartz cell was used as the electrolyte. A high-pressure 500 W Hg lamp was used as the light source in the photoelectrochemical measurements.

Acknowledgements

This work was supported by the Core Research of Evolutional Science & Technology (CREST) of the Japan Science and Technology Agency, Grant-in-Aid for Young Scientists(B) (No. 23710131), and Grant-in-Aid for Scientific Research(A) (No. 23245036). We thank Prof. Iwamoto for performing TEM analysis.

Received: September 18, 2012
Revised: November 13, 2012
Published online: January 18, 2013

[1] X. Peng, L. Manna, W. Yang, J. Wickham, E. Scher, A. Kadavanich, A. P. Alivisatos, *Nature* **2000**, *404*, 59.
[2] P. Alivisatos, *Nat. Biotechnol.* **2004**, *22*, 47.
[3] R. Makiura, T. Yonemura, T. Yamada, M. Yamauchi, R. Ikeda, H. Kitagawa, K. Kato, M. Takata, *Nat. Mater.* **2009**, *8*, 476.
[4] Y. Yamamoto, T. Miura, M. Suzuki, N. Kawamura, H. Miyagawa, T. Nakamura, K. Kobayashi, T. Teranishi, H. Hori, *Phys. Rev. Lett.* **2004**, *93*, 116801.
[5] M. Suda, N. Kameyama, M. Suzuki, N. Kawamura, Y. Einaga, *Angew. Chem. Int. Ed.* **2008**, *47*, 160.
[6] S. S. Rao, S. N. Jammalamadaka, A. Stesmans, V. V. Moshchalkov, J. V. Tol, D. V. Kosynkin, A. Higginbotham-Duque, J. M. Tour, *Nano Lett.* **2012**, *12*, 1210.
[7] S. K. Saha, M. Baskey, D. Majumdar, *Adv. Mater.* **2010**, *22*, 5531.
[8] L. Pisani, J. A. Chan, B. Montanari, N. M. Harrison, *Phys. Rev. B* **2007**, *75*.
[9] M. Venkatesan, C. B. Fitzgerald, J. M. D. Coey, *Nature* **2004**, *430*, 630.
[10] J. M. D. Coey, *Solid State Sci.* **2005**, *7*, 660.
[11] A. Sundaresan, R. Bhargavi, N. Rangarajan, U. Siddesh, C. N. R. Rao, *Phys. Rev. B* **2006**, *74*.
[12] R. Podila, W. Queen, A. Nath, J. T. Arantes, A. L. Schoenhalz, A. Fazzio, G. M. Dalpian, J. He, S. J. Hwu, M. J. Skove, A. M. Rao, *Nano Lett.* **2010**, *10*, 1383.
[13] S. Z. Deng, H. M. Fan, M. Wang, M. R. Zheng, J. B. Yi, R. Q. Wu, H. R. Tan, C. H. Sow, J. Ding, Y. P. Feng, K. P. Loh, *ACS Nano* **2010**, *4*, 495.
[14] C. Guglieri, M. A. Laguna-Marco, M. A. García, N. Carmona, E. Céspedes, M. García-Hernández, A. Espinosa, J. Chaboy, *J. Phys. Chem. C* **2012**, *116*, 6608.
[15] A. Hernando, M. A. García, *J. Nanopart. Res.* **2011**, *13*, 5595.
[16] X. Xu, C. Xu, J. Dai, J. Hu, F. Li, S. Zhang, *J. Phys. Chem. C* **2012**, *116*, 8813.
[17] D. X. Xia, W. H. Zhang, F. Y. Xie, J. Chen, J. B. Xu, *J. Nanosci. Nanotechnol.* **2011**, *11*, 10557.
[18] S. Banerjee, M. Mandal, N. Gayathri, M. Sardar, *Appl. Phys. Lett.* **2007**, *91*.
[19] C. Guglieri, J. Chaboy, *J. Phys. Chem. C* **2010**, *114*, 19629.
[20] J. F. Liu, E. Z. Liu, H. Wang, N. H. Su, J. Qi, J. Z. Jiang, *Nanotechnology* **2009**, *20*.
[21] S. Majumder, D. Paramanik, A. Gupta, S. Varma, *Appl. Surf. Sci.* **2009**, *256*, 513.
[22] C. S. Ong, T. S. Herng, X. L. Huang, Y. P. Feng, J. Ding, *J. Phys. Chem. C* **2012**, *116*, 610.
[23] B. Panigrahy, M. Aslam, D. S. Misra, M. Ghosh, D. Bahadur, *Adv. Funct. Mater.* **2010**, *20*, 1161.
[24] A. L. Schoenhalz, J. T. Arantes, A. Fazzio, G. M. Dalpian, *Appl. Phys. Lett.* **2009**, *94*.
[25] Q. Wang, Q. Sun, P. Jena, *J. Chem. Phys.* **2008**, *129*.
[26] G. Xing, D. Wang, J. Yi, L. Yang, M. Gao, M. He, J. Yang, J. Ding, T. C. Sum, T. Wu, *Appl. Phys. Lett.* **2010**, *96*.
[27] M. A. Garcia, J. M. Merino, E. F. Pinel, A. Quesada, J. De La Venta, M. L. R. González, G. R. Castro, P. Crespo, J. Llopis, J. M. González-Calbet, A. Hernando, *Nano Lett.* **2007**, *7*, 1489.
[28] J. I. Hong, J. Choi, S. S. Jang, J. Gu, Y. Chang, G. Wortman, R. L. Snyder, Z. L. Wang, *Nano Lett.* **2012**, *12*, 576.
[29] A. L. Schoenhalz, J. T. Arantes, A. Fazzio, G. M. Dalpian, *J. Phys. Chem. C* **2010**, *114*, 18293.
[30] O. Altuntasoglu, Y. Matsuda, S. Ida, Y. Matsumoto, *Chem. Mater.* **2010**, *22*, 3158.
[31] L. Zhang, H. Huang, *Appl. Phys. Lett.* **2007**, *90*.
[32] C. L. Freeman, F. Claeyssens, N. L. Allan, J. H. Harding, *Phys. Rev. Lett.* **2006**, *96*.
[33] H. Cölfen, M. Antonietti, *Angew. Chem. Int. Ed.* **2005**, *44*, 5576.
[34] X. Zhang, H. Yin, X. Cheng, H. Hu, Q. Yu, A. Wang, *Mater. Res. Bull.* **2006**, *41*, 2041.
[35] Y. Arai, D. L. Sparks, *J. Colloid Interface Sci.* **2001**, *241*, 317.